J Nanopart Res (2023) 25:69
https://doi.org/10.1007/s11051-023-05717-2

RESEARCH PAPER

Fabrication of electrodes by deposition of lead clusters from the Matrix Assembly Cluster Source (MACS) into porous carbon paper for electrocatalysis

E. Kazimierska · Y. Niu · J. McCormack · C. Tizaoui · Richard J. Cobley · R. E. Palmer

Received: 29 August 2022 / Accepted: 12 March 2023 / Published online: 28 March 2023

Abstract The scaling up of the intensity of beams of atomic clusters (nanoparticle beams) creates a new route to the fabrication of functional nanostructured materials. A challenge is to present, to the directed beam, high surface areas of the desired support material, for decoration by the clusters at local sub-monolayer densities. Then, the clusters and their properties can be preserved. Here we employ the Matrix Assembly Cluster Source (MACS) to demonstrate and characterise the deposition of lead clusters, with size of order 2 nm, into planar sheets of porous carbon paper, a material employed in electrode fabrication. We find that clusters are deposited to a depth comparable with the pore size of the carbon, ~ 50 µm, giving rise to a metal loading of ~ 0.05 mg cm^{-2} of carbon paper. The functionality of the nanocomposite film so created is demonstrated by its use as an electrode for the electrochemical generation of oxidising species suitable for water purification.

E. Kazimierska · C. Tizaoui
Water and Resources Recovery Research Lab, Department of Chemical Engineering, Swansea University, Bay Campus, Fabian Way, Swansea SA1 8EN, UK

Y. Niu (✉) · J. McCormack · R. J. Cobley · R. E. Palmer
Nanomaterials Lab, Department of Mechanical Engineering, Swansea University, Bay Campus, Fabian Way, Swansea SA1 8EN, UK
e-mail: yubiao.niu@swansea.ac.uk

Keywords Nanoparticle · Clusters · Carbon paper · Cluster source · Electrochemical · Nanocomposite film

Introduction

Nanoparticles are assemblies of atoms or molecules with sizes in the range 1–100 nm [1, 2]. The ability to tailor the unique chemical or physical properties of the nanoparticles has enabled them to be used in a wide spectrum of applications, such as catalysis [3, 4], medicine [5, 6] and photonics [7, 8]. Many approaches have been explored for the production of nanoparticles with well controlled size and composition, including chemical [9, 10], physical [11, 12] and biological [13, 14] methods. Cluster (nanoparticle) beam deposition is a physical technique recognised as a promising method for environmentally clean ("green") nanoparticle production [2, 15].

The directional and ballistic nature of the cluster beam generated by a cluster source presents challenges for coating the desired cluster support in an even way. Scaled-up cluster beam sources are now available [16, 17], which are capable of depositing fractions of a gram of clusters per hour onto a support to create functional materials such as catalysts. To take full advantage of these new instruments, such as the Matrix Assembly Cluster Source [18, 19], we must learn to present to the directed beam large surface areas of the support material. A successful

innovation has been to agitate or stir a powder while it is coated (from above) by the cluster beam. Several examples of heterogeneous catalysis with such cluster-decorated powder materials have been reported [20–23]. A problem of cluster deposition into powders is that the impact parameters of the cluster-surface collision vary, because each powder particle presents a curved surface at uncontrolled angle to the incoming cluster. If the fate of the cluster—in terms of its final shape on, and diffusion across, the surface—depends on the precise landing site and angle, non-uniform cluster coverage and morphology may result. Presenting to the cluster beam a planar surface at normal incidence overcomes this problem, but obviously limits the area that can be decorated, if the preservation of individual clusters is required. Scanning of the planar support to be coated underneath the beam resolves these issues [24]. A third approach, as demonstrated herein, is to present to the beam a porous support material whose microscopic surface area, available for cluster binding, is enormously higher than the macroscopic projected surface area of the material. Porous carbon paper [25] is one of many such examples. Since nanocomposite layers—consisting of nanoparticles dispersed by chemical means within such porous supporting frameworks—already have important applications in, e.g. the chemicals and energy sectors [26, 27], the demonstration of cluster beam deposition into porous materials has obvious practical relevance as well as fundamental interest.

Methods and discussions

The deposition of lead (Pb) clusters into porous carbon paper was accomplished with the Matrix Assembly Cluster Source (MACS) technique. The carbon paper (Sigracet 29 AA, SGL Carbon) used in this work has a thickness of about 200 µm, with a mean pore size of about 50-µm diameter. The porosity of the carbon paper is 80% according to the specification sheet of the supplier. The details of this cluster beam technique have been described previously [21]. The Pb clusters were formed and deposited onto carbon paper in the MACS deposition chamber. An oxygen-free copper support was cooled to around 20 K by a closed-loop helium cryocooler, then a solid cryomatrix of Pb and argon (Ar) atoms was produced on the surface of the copper support, by evaporating Pb atoms and dosing Ar gas at the same time. After the formation of the matrix, an Ar^+ ion beam (1.1 kV, 15–20 mA) was employed to sputter the matrix, creating a beam of Pb clusters, which were directly deposited onto the carbon paper. The clusters are formed by collision cascades in the matrix. The carbon paper (circular shape) with diameter 10 cm was introduced into the deposition chamber from a load-lock chamber prior to Pb cluster deposition from the matrix; we refer to the result as "Pb-C" paper.

During the formation of the matrix, a quartz crystal microbalance was used to measure the metal evaporation rate in the matrix, 10 Å/s. The Ar dosing pressure was set (4.5×10^{-4} mbar) to achieve a metal loading in the matrix of ~ 4% by number of atoms. The production of Pb cluster beam was achieved by sputtering the matrix with Ar^+ ion beam (1.1 kV, 15–20 mA). The carbon paper was rotated on a stage throughout entirety of the deposition to achieve uniform deposition. In order to achieve a decent metal loading on the support, a deposition time of 1 h was used. To measure the amount deposited, quartz crystal microbalances were used. We estimate that the total amount of Pb clusters deposited on the carbon papers was about 1.45 mg for the scanning transmission electron microscopy (STEM) study and 4.40 mg for the scanning electron microscopy (SEM) and electrochemical studies, i.e. 0.018mg/cm^2 and 0.056mg/cm^2, respectively.

The microscopic morphology of the C-paper before and after deposition with Pb clusters was characterised with SEM. Chemical information on the Pb-C paper was revealed with EDX analysis. SEM images of the bare carbon paper support and Pb-C paper are shown in Fig. 1A and B, respectively. The carbon substrate was characterised as interconnected carbon fibres with an average thickness of 7 µm as well as carbon particles and flakes with a diameter ranging from 10 to 30 µm, randomly scattered over the surface. Changes in the surface morphology of the carbon fibres as a result of Pb coating confirm that Pb was successfully deposited. Additionally, from magnified sections of the SEM images, the surface of the pristine C-paper appeared smooth whereas the surface of the Pb-C paper presented to the cluster beam became rougher.

For cross-sectional analysis, the samples were cut with a surgical blade and mounted vertically on the SEM sample holder. The cross-sectional SEM and

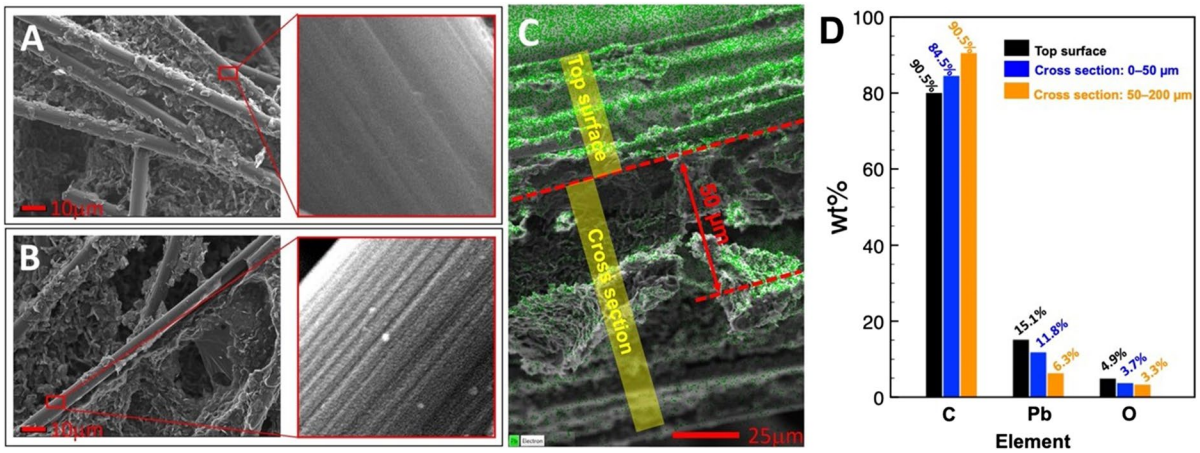

Fig. 1 **A** SEM images of bare carbon paper and **B** of Pb deposited into the carbon paper. **C** EDX mapping of a cross-section of Pb-C paper, showing the Pb clusters are mainly located in the upper section of the carbon paper with a depth of 50 µm. **D** Average element concentration in weight % of C, Pb and O from the different section of Pb-C paper: top surface, cross-section within 0-50 µm depth and cross-section within 50–200-µm depth

EDX analysis of the Pb-C paper, Fig. 1C, showed that the ~ 200-µm-thick carbon film was built of interconnected carbon fibres and particles as described, with pores evident throughout the material, providing tunnels for the directed Pb clusters to penetrate into. The upper cross-section (0–50-µm depth) shown in Fig. 1C showed Pb cluster deposition throughout the depth analysed, ~ 50 µm from the top surface of the C-paper, which is comparable with the pore size. The lower cross-section (50–200-µm depth), showing a reduced amount of Pb within the C-paper; this section had a depth ~ 150 µm. EDX analysis of the Pb-C paper shown in Fig. 1D indicates that the concentration of Pb decreases from top surface to cross-section. ~ 54.5% of the total amount of Pb infiltrated the paper and settled on the inner carbon fibres.

The stability of the Pb-C paper was also evaluated by EDX analysis. Samples of carbon paper with deposited Pb clusters were immersed in de-ionised water and also 0.5 M H_2SO_4 for 16 h. After this time, the amount of Pb in the carbon paper was reduced by 81% and 97% for DI water and the acid, respectively, suggesting rather weak adhesion of Pb to the carbon paper matrix.

A small section with a diameter of ~ 3 mm was cut from the Pb-carbon paper for scanning transmission electron microscopy (STEM) imaging. The STEM imaging was performed using a Thermo Scientific Talos F200X Transmission Electron Microscope operating at 200 kV in the high-angle annular dark-field (HAADF) mode. The images were taken from the ultrathin area located on the carbon flake of the carbon paper. It can be seen from Fig. 2a that the surface of the Pb-carbon paper is covered with sphere-like structures. Figure 2b shows that those sphere-like structures are decorated with small Pb clusters. The HAADF contrast indicates that the spheres themselves are carbon rather than Pb, as the small Pb clusters would not be visible if the spheres were Pb.

In order to study the size of the structures assigned to carbon spheres and Pb clusters, their projected surface areas were measured and converted into diameters. One hundred forty-right and two hundred sixty carbon sphere and Pb nanoparticles were measured for the size distributions of Fig. 2c and d. The carbon structures have a mean diameter of 15.9 nm, while the Pb clusters have a mean diameter of 2.1 nm. The porous structure of the carbon paper can allow the cluster beam to penetrate into a certain depth, which is confirmed by the SEM-EDS mapping of the cross-section shown in Fig. 1. The uniform dispersion and the narrow size distribution of Pb clusters indicate there is no further diffusion and aggregation for Pb clusters after landing on the support.

The functionality of the nanocomposite material was demonstrated in a preliminary fashion by experiments in which the Pb-C paper was used as an electrode (anode) in an electrochemical flow cell reactor,

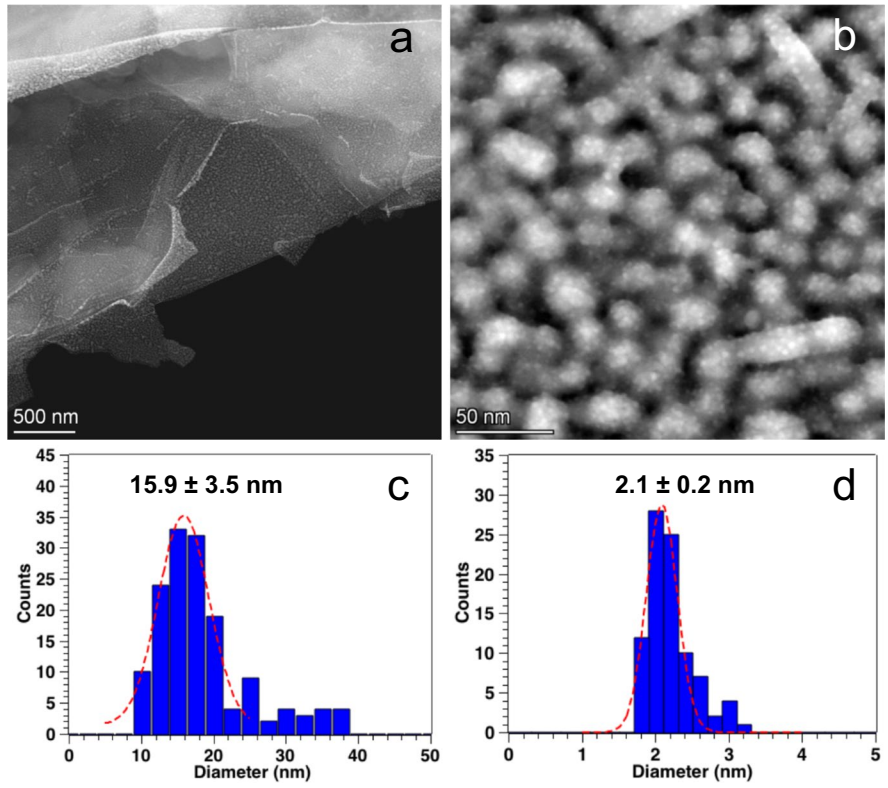

Fig. 2 HAADF-STEM images of carbon paper after Pb cluster deposition under low magnification (**a**) and high magnification (**b**). The carbon paper presents sphere-like structures with a mean diameter of 15.9 nm (**c**), and those spheres are decorated with Pb clusters with a mean diameter of 2.1 nm

to generate reactive oxidative species (ROS) in aqueous solution, as tested through the degradation of potassium indigo trisulphonate. With a constant voltage of 10 V applied for 60 min, the potassium indigo trisulphonate electrolyte was allowed to circulate in the cell at a constant rate of 2.5 L/h. The absorbance due to the blue indigo trisulphonate indicator (wavelength 600 nm) gradually decreased as a result of oxidation by ROS produced in the cell (e.g. hydroxy radicals and ozone) (Fig. 3). The colour change of the

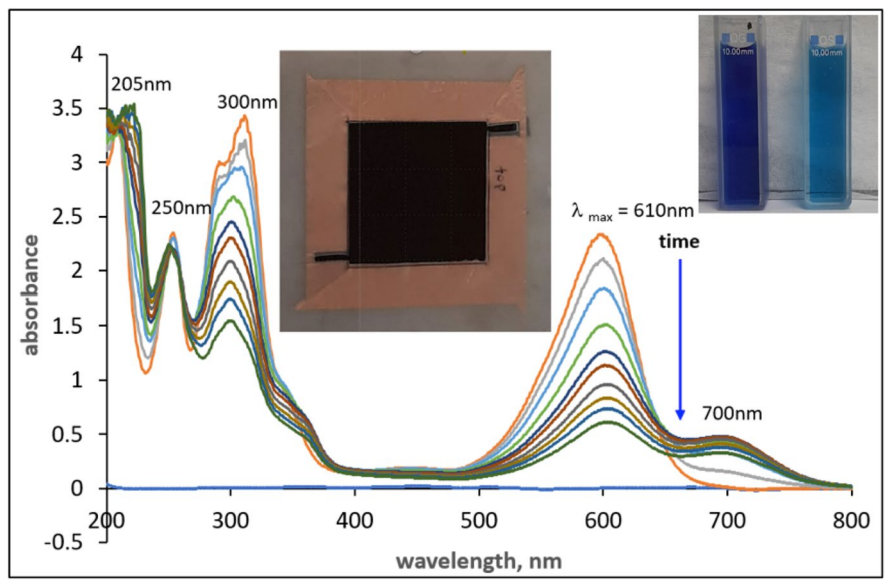

Fig. 3 Gradual degradation of indigo dye on a Pb-C paper anode monitored by changes in the optical absorbance measured after 2, 5, 10, 20 35, 45, 60, 75, 90 and 120 min. Inset in the middle shows the Pb-C carbon paper mounted as an electrode and inset in the upper right corner shows the colours of original indigo stock solution (left) and indigo solution after 120 min of electrochemical decomposition at 10V on Pb-C paper electrode (right)

dye solution is indicative that such species were generated in the reaction cell [28, 29]. At the molecule level, the double bonds between carbon atoms (> C = C <) in the indigo molecule break when exposed to oxidative species and the carbon atoms are oxidised (two > C = O entities are created). The products are colourless. The reaction is below:

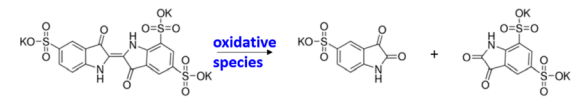

Regarding the specifics of the UV/Vis spectra, the characteristic absorbance band for indigo is at 600 nm. The other three peaks observed in the UV region correspond to structural features of the dye: the peak at 300 nm is related to the amino group, that at 250 nm is attributed to the carbonyl group and the peak at 205 nm corresponds to the resonance of the aromatic ring. The peak which grows with time at approximately 700 nm could be due to interaction between the dye and metal ions (e.g. Pb(II) or Cu(II)) to form a metal-dye complex that absorbs at higher wavelength [30]. Pb(II) could be formed by dissolution of the Pb clusters into electrolyte and Cu(II) could be formed by dissolution of the conductor. In order to prevent the dissolution of Pb from support to solution, an oxide support can be used to anchor the Pb cluster in place.

Conclusions and outlook

In this work, Pb clusters with an average diameter of ~ 2 nm were fabricated with the MACS technique and deposited into porous C-paper. Both STEM and SEM studies together with EDX mapping confirm the successful deposition of Pb clusters to form the nanocomposite Pb-C paper system. The EDX analysis indicates that the Pb clusters are deposited to a depth into the carbon paper comparable with the pore size of the carbon paper, ~ 50 µm. The Pb-C paper was tested as an electrode for the electrochemical generation of highly reactive oxidative species in an electrochemical flow cell reactor. The Pb-C paper showed initial activity but deactivated on the timescale of 10 s, attributed to the dissolution of Pb clusters into electrolyte. Future work will need to address the adhesion/anchoring of the clusters to the fibres of the host material. Most significantly, this study has demonstrated a method of presenting a high surface area host material to an intense directed beam of sub-10-nm clusters. The method has few steps and may be competitive with chemical approaches.

Acknowledgements We thank Morris Mathews for his support of the cluster deposition with the MACS. We also acknowledge the support provided by the AIM Facility of Swansea University, which was funded in part by the EPSRC (EP/M028267/1), the European Regional Development Fund through the Welsh Government (80708) and the Welsh Government Sêr Cymru programme. We are grateful for the financial support of the work by Sêr Cymru II – WEFO ERDF Programme (80761) and the UK's Global Challenges Research Fund via the Swansea University institutional grant and by EPSRC (Grant Reference No. EP/ K006061/2). A patent application (pending) based on part of the research work is in place.

Compliance with ethical standards

Conflict of interest The authors declare that they have no conflict of interest.

References

1. Kreyling WG, Semmler-Behnke M, Chaudhry Q (2010) A complementary definition of nanomaterial. Nano Today 5:165–168
2. Palmer RE, Cai RS, Vernieres J (2018) Synthesis without solvents: the cluster (nanoparticle) beam route to catalysts and sensors. Accounts Chem Res 51:2296–2304
3. Astruc D (2020) Introduction: nanoparticles in catalysis. Chem Rev 120:461–463
4. Escalera-Lopez D, Niu YB, Park SJ, Isaacs M, Wilson K, Palmer RE, Rees NV (2018) Hydrogen evolution enhancement of ultra-low loading, size-selected molybdenum

sulfide nanoclusters by sulfur enrichment. Appl Catal B-Environ 235:84–91
5. Lin WB (2015) Introduction: nanoparticles in medicine. Chem Rev 115:10407–10409
6. Yadid M, Feiner R, Dvir T (2019) Gold nanoparticle-integrated scaffolds for tissue engineering and regenerative medicine. Nano Lett 19:2198–2206
7. Marago OM, Jones PH, Gucciardi PG, Volpe G, Ferrari AC (2013) Optical trapping and manipulation of nanostructures. Nat Nanotechnol 8:807–819
8. Mao P, Liu CX, Niu YB, Qin YY, Song FQ, Han M, Palmer RE, Maier SA, Zhang S (2021) Disorder-induced material-insensitive optical response in plasmonic nanostructures: vibrant structural colors from noble metals. Adv Mater 33:8
9. Kimling J, Maier M, Okenve B, Kotaidis V, Ballot H, Plech A (2006) Turkevich method for gold nanoparticle synthesis revisited. J Phys Chem B 110:15700–15707
10. Heuer-Jungemann A, Feliu N, Bakaimi I, Hamaly M, Alkilany A, Chakraborty I, Masood A, Casula MF, Kostopoulou A, Oh E et al (2019) The role of ligands in the chemical synthesis and applications of inorganic nanoparticles. Chem Rev 119:4819–4880
11. Pratontep S, Carroll SJ, Xirouchaki C, Streun M, Palmer RE (2005) Size-selected cluster beam source based on radio frequency magnetron plasma sputtering and gas condensation. Rev Sci Instrum 76:9
12. Liao TW, Yadav A, Ferrari P, Niu YB, Wei XK, Vernieres J, Hu KJ, Heggen M, Dunin-Borkowski RE, Palmer RE et al (2019) Composition-tuned pt-skinned ptni- bimetallic clusters as: highly efficient methanol dehydrogenation catalysts. Chem Mat 31:10040–10048
13. Singh P, Kim YJ, Zhang DB, Yang DC (2016) Biological synthesis of nanoparticles from plants and microorganisms. Trends Biotechnol 34:588–599
14. Thakkar KN, Mhatre SS, Parikh RY (2010) Biological synthesis of metallic nanoparticles. Nanomed-Nanotechnol Biol Med 6:257–262
15. Wegner K, Piseri P, Tafreshi HV, Milani P (2006) Cluster beam deposition: a tool for nanoscale science and technology. J Phys D Appl Phys 39:R439–R459
16. Palmer RE, Cao L, Yin F (2016) Note: Proof of principle of a new type of cluster beam source with potential for scale-up. Rev Sci Instrum 87:3
17. Sanzone G, Yin JL, Sun HL (2021) Scaling up of cluster beam deposition technology for catalysis application. Front Chem Sci Eng 15:1360–1379
18. Spadaro MC, Cao L, Terry W, Balog R, Yin F, Palmer RE (2020) Size control of au nanoparticles from the scalable and solvent-free matrix assembly cluster source. J Nanopart Res 22:6
19. Ellis PR, Brown CM, Bishop PT, Yin JL, Cooke K, Terry WD, Liu J, Yin F, Palmer RE (2016) The cluster beam route to model catalysts and beyond. Faraday Discuss 188:39–56
20. Xu JY, Murphy S, Xiong DH, Cai RS, Wei XK, Heggen M, Barborini E, Vinati S, Dunin-Borkowski RE, Palmer RE et al (2018) Cluster beam deposition of ultrafine cobalt and ruthenium clusters for efficient and stable oxygen evolution reaction. ACS Appl Energ Mater 1:3013–3018
21. Cai RS, Martelli F, Vernieres J, Albonetti S, Dimitratos N, Tizaoui C, Palmer RE (2020) Scale-up of cluster beam deposition to the gram scale with the matrix assembly cluster source for heterogeneous catalysis (catalytic ozonation of nitrophenol in aqueous solution). ACS Appl Mater Interfaces 12:24877–24882
22. Cai RS, Cao L, Griffin R, Chansai S, Hardacre C, Palmer RE (2020) Scale-up of cluster beam deposition to the gram scale with the matrix assembly cluster source for heterogeneous catalysis (propylene combustion). AIP Adv 10(5)
23. Cai RS, Malta G, Haigh SJ, Hutchings GJ, Freakley SJ, Palmer RE (2020) Gas-phase deposition of gold nanoclusters to produce heterogeneous glycerol oxidation catalysts. ACS Appl Nano Mater 3:4997–5001
24. Santaniello T, Milani P (2020) 12 - additive nano-manufacturing of 3d printed electronics using supersonic cluster beam deposition. In: Milani P, Sowwan M (eds) Frontiers of nanoscience, vol 15. Elsevier, pp 313–333
25. Wang Y, Wang CY, Chen KS (2007) Elucidating differences between carbon paper and carbon cloth in polymer electrolyte fuel cells. Electrochim Acta 52:3965–3975
26. Liu XH, Ouyang MZ, Orzech MW, Niu YB, Tang WQ, Chen JY, Marlow MN, Puhan D, Zhao Y, Tan R et al (2020) In-situ fabrication of carbon-metal fabrics as free-standing electrodes for high-performance flexible energy storage devices. Energy Storage Mater 30:329–336
27. Kakhki RM (2019) A review to recent developments in modification of carbon fiber electrodes. Arab J Chem 12:1783–1794
28. Kim J, Korshin GV (2008) Examination of in situ generation of hydroxyl radicals and ozone in a flow-through electrochemical reactor. Ozone-Sci Eng 30:113–119
29. Lai J, Foster JE (2019) Plasma-driven reactive species production and transport in a 2-d discharge cell. IEEE Trans Plasma Sci 47:4422–4427
30. Zanoni TB, Cardoso AA, Zanoni MVB, Ferreira AAP (2010) Exploratory study on sequestration of some essential metals by indigo carmine food dye. Braz J Pharm Sci 46:723–730